arXiv:1505.05145v1 [astro-ph.SR] 19 May 2015

A Compact Circumstellar Shell as the Source of High–velocity Features in SN 2011fe

Brian W. Mulligan
The University of Texas at Austin
`bwmulligan@astro.as.utexas.edu`
and

J. Craig Wheeler
The University of Texas at Austin
`wheel@astro.as.utexas.edu`

May 21, 2015

ABSTRACT

High–velocity features (HVF), especially of Ca II, are frequently seen in Type Ia supernovae observed prior to B–band maximum (Bmax). These HVF start at more than $25,000\ \mathrm{km\,s^{-1}}$ in the days after first light, and slow to about $18,000\ \mathrm{km\,s^{-1}}$ near Bmax. To recreate the Ca II near–infrared triplet (CaNIR) HVF in SN 2011fe, we consider the interaction between a Type Ia supernova and a compact circumstellar shell, employing a hydrodynamic 1–D simulation using FLASH. We generate synthetic spectra from the hydrodynamic results using `syn++`. We show that the CaNIR HVF and its velocity evolution is better explained by a supernova model interacting with a shell than a model without a shell, and briefly discuss the implications for progenitor models.

Subject headings: supernovae: general — supernovae: individual (SN 2011fe) — line: formation — line: profiles

1. Introduction

Type Ia supernovae (SN Ia) provide a fundamental tool for our understanding of the history of the universe. SN Ia are 'standardizable candles' used to explore the expansion of the universe as well as the chemical enrichment of galaxies (Riess et al. 1998; Perlmutter et al. 1999; Tsujimoto & Shigeyama 2012). The configuration of the progenitor system and the cause of the explosion remain elusive. Observations of SN 2011fe within the first day after the explosion have shown that any optically thick material was within $0.1R_\odot$ of the exploding star prior to the explosion (Nugent et al. 2011; Piro & Nakar 2014). Spectroscopy of SN Ia in the first days and weeks after the explosion also reveal high–velocity features (HVF) in Ca II, Si II, and other ions (Hatano et al. 1999; Parrent et al. 2012; Marion et al. 2013). The HVF has a velocity $\gtrsim 25,000\ \mathrm{km\,s^{-1}}$ at 15-18 days before B–band maximum (Bmax) and slows to a plateau of about $18,000$ by Bmax. The photosphere also starts at high velocity and moves to lower velocities over the same interval, but the HVF consistently remain $\gtrsim 7,000\ \mathrm{km s^{-1}}$ faster than the photospheric velocity features (PVF) (Marion et al. 2013; Maguire et al. 2014; Silverman et al. 2015). Ca II HVF appear in over 90% of normal SN Ia (Mazzali et al. 2005; Childress et al. 2014; Maguire et al. 2014; Silverman et al. 2015) and show significant polarization (Wang et al. 2003), indicating that the material has a high covering factor and is asymmetric.

The source of the high-velocity material will give insight to the nature of the progenitor system or mechanism by which the explosion is initiated; understanding both of these is necessary to control the systematics in the use of SN Ia as cosmological probes. Previous suggestions for the source of the high–velocity material include plumes of partially burned ejecta (Wang et al. 2003), buoyant bubbles due to a gravitationally confined detonation (Kasen & Plewa 2005), or interaction with a circumstellar medium (CSM) with a total mass of high-velocity material of about $0.02\,M_{\odot}$ and solar abundance (Gerardy et al. 2004; Quimby et al. 2006). These models consider HVF velocity at the time near or after Bmax, when the HVF are in the asymptotic phase and are fading. It is necessary to explain the full evolution of the velocity and strength throughout the period the HVF is detectable in order to understand the source.

In this letter, we consider the interaction between a circumstellar shell (CSS) of mass $0.005M_{\odot}$ located within $0.3\,R_{\odot}$ of the center of the explosion and compare this model to a supernova with no CSS sources of the HVF. We concentrate on the Ca II near-infrared triplet (CaNIR) in SN 2011fe between $-16.5\,$d and $+2.9\,$d. In §2 we describe the hydrodynamic methods used, the SN model (§2.1), and the CSS (§2.2). In §3 we discuss the methods used for generating synthetic spectra from the hydrodynamic results. We present the results in §4, and summarize our conclusions in §5.

2. Hydrodynamics

We use FLASH 4.1 (Fryxell et al. 2000) with multi–pole gravity, 1–D spherical geometry, the Helmholtz equation of state (EOS) (Timmes & Arnett 1999) for the supernova–only model and the gamma law EOS for the model including the CSS. The simulation volume has the supernova at the center and a radius of 10^{12} cm, with a minimum resolution of 4.2×10^{6} cm per zone. The multi–species unit is used to track H, ^{3}He, ^{4}He, ^{12}C, ^{16}O, ^{24}Mg, ^{32}Si, and ^{56}Ni. The model is evolved to about 50s after the explosion at which time the the shock has fully propagated through the shell (when it is included) and both the ejecta and shell are in or near the free expansion phase. The choice of end point and EOS for a given model is governed by the density floor in the Helmholtz EOS and the desire to have similar end times for each model.

2.1. Explosion Model

The explosion models are those of Gamezo et al. (2005) delayed-detonation models `b` and `c`. We maintain the resolution of the original model, which has a maximum radius of 5.4×10^{8} cm resolved into 128^{3} zones ($4.2\times10^{6}\,$cm per zone). We use spherical averaging to reduce the model from 3–D to 1–D. The model provides C, O, Mg group, Si group, and Fe group abundances for each zone. Exterior to the ejecta we apply a CSM with density 10^{-9} g cm^{-3} and temperature of $20,000\,$K.

2.2. Circumstellar shell model

We have explored a range in masses and density distributions for the shell. These results that will be reported in a forthcoming paper (Mulligan & Wheeler in preparation). For this work, we use a shell with inner radius 7×10^{8} cm and outer radius $2\times10^{10}\,$cm ($0.3\,R_{\odot}$), a total mass of $0.005\,M_{\odot}$ with a density profile that decreases linearly outward, and a temperature of $30,000\,$K. Exterior to the shell, the CSM parameters are applied as described in the previous subsection. For the hydrodynamic simulation, we assume a hydrogenic shell with solar abundances. Total He abundance in the shell is taken to be solar, but we enhance the ^{3}He by 10% to act as a tracer.

3. Spectral synthesis

We use the result of the hydrodynamic simulation to generate an optical depth profile as a function of velocity. The line optical depth for an individual zone is computed using the Sobolev approximation then binned with zones having a similar velocity. We assume excitation temperature is constant over the line–generating regions in the ejecta and shell. We define scaling factors C^{E} and C^{S} to account for the fraction of Ca II relative to all Si group elements in the ejecta and Ca II abundance by mass within the shell, respectively.

We use `syn++` (Thomas et al. 2011), modified to allow an arbitrary optical depth as a function of velocity, to generate the synthetic spectra. When generating the spectra, the time after explosion, photospheric temperature and velocity, and the abundance scale factors C^E and C^S are free parameters. The photospheric velocity and temperature set the minimum velocity of the photospheric line-generating region and the shape of the continuum, respectively. We adopt a lower limit to the temperature of the photosphere of $8,000$ K. The effects of the excitation temperature, ion mass fraction, and time after explosion are degenerate. We fix the excitation temperature to $10,000$K and the time after explosion to 1 day and vary only the ion mass fraction to represent the value of these combined parameters. The abundance scale factors are limited such that the total optical depth stays below 10^4 to prevent unobserved Ca II features from appearing in the synthetic spectra, e.g. a $\lambda5020$ doublet.

We fit the model spectra to the observed spectra SN 2011fe from Parrent et al. (2012) over the period -16.54 d to $+2.87$ d. For fitting purposes, normalization factors N^s and N^o are computed such that

$$\int_{\lambda_l}^{\lambda_u} N^s \mathcal{F}^s_\lambda d\lambda = \int_{\lambda_l}^{\lambda_u} N^o \mathcal{F}^o_\lambda d\lambda = 0.5, \qquad (1)$$

where $\mathcal{F}_\lambda$ is the specific flux density from either our synthetic spectra ($\mathcal{F}^s_\lambda$) or observed spectra ($\mathcal{F}^o_\lambda$). We have chosen the bounds to be $\lambda_l = 4500$ Å and $\lambda_u = 9000$ Å to cover the majority of the optical spectrum. A multi-variable simplex fitting routine is used to minimize the variance $\sigma^2 = \langle (N^s\mathcal{F}^s_\lambda - N^o\mathcal{F}^o_\lambda)^2 \rangle$ over the range 7750Å and 8400 Å, which covers most of the CaNIR absorption feature. The CaNIR feature is chosen because it is the most conspicuous HVF, and it allows a fit without concern of blending with Si, as may occur in the Ca H&K feature (Maguire et al. 2012; Foley 2013; Silverman et al. 2015). Details of the dynamic models and line–fitting procedure will be given in Mulligan & Wheeler (in preparation).

4. Results and discussion

Synthetic spectra for the models are shown in Figures 1 and 2 for the case of the supernova–only model (SN–O) and supernova with a shell of mass $0.005\,M_\odot$ (SN+S), respectively. These figures also present the observed spectra of SN 2011fe from Parrent et al. (2012). The photospheric velocity and temperature, abundance scaling factors (C^S and C^E), and variance of the fit (σ) are listed in Table 1. The photosphere velocity and temperature are based only on the fit to the CaNIR feature and are therefore not strong indicators of the actual photospheric parameters; fitting of additional absorption features will give more reliable values. In the discussion below, phase is based on Bmax on JD 2,455,814.4 (Vinkó et al. 2012).

The SN+S model tends to produce a better fit to the width of the CaNIR feature over the entire period studied, although the variance usually differs by only about 0.1 between the SN–O and SN+S models. The largest exception is for the earliest available spectrum (-16.54 d), when the SN+S model is a better fit by about 0.5 dex than the SN–O model. This is also apparent by visually inspecting the resulting spectra: the SN–O model leaves gaps both red–ward and blue–ward of the feature minimum. Part of the reason the earliest fit of the SN+S model is better than the remainder of the fits is the success in capturing the whole of the P Cygni peak; with the exception of -10.54d, there is excess flux at the peak in the observations that the models do not reproduce. This is due to the choice of a fixed upper limit for fitting at 8400 Å, which does capture the peak on -16.54 d, but is blue–ward of the peak at all later times. From visual inspection, the fit tends to result in the flux near 8400 Å matching the observed value but with an incorrect slope. A dynamically chosen upper wavelength limit for the fit would improve this result; this will be incorporated in future work.

At the earliest times in the SN+S model, the photosphere lies in the shell rather than in the ejecta. The contact discontinuity between ejecta and shell material lies at $20,880$ km s^{-1}. On -16.54 d our fit finds a photosphere velocity of $21,660$ km s^{-1}, which is within the shell; one day later the photosphere lies at $20,820$ km s^{-1}, just inside the ejecta. This results in no measurable PVF in our model in these first two epochs. By -13.21 d and later, the photosphere has receded into or below the freshly synthesized Ca, giving distinct PVF and HVF due to the ejecta and shell, respectively. At -7.27 d and later, the shell has become optically thin to CaNIR and the HVF due to the shell becomes very weak.

There is a feature near 8000 Å in both the observed and the SN+S model spectra that is missing from the SN–O model spectra. This feature is due exclusively to absorption within the ejecta in the SN+S model. The lack of such a feature in the SN–O model suggests that it is a result of the interaction between the ejecta and shell. We have tested simplified models of a density enhancement at the reverse shock in the ejecta that do not immediately account for this interaction feature (IF). We will further explore the physical origin of the IF in our upcoming paper, Mulligan & Wheeler (in preparation).

4.1. Velocity evolution

Generating spectra with C^S or C^E set to a small value (10^{-20}) allows us to individually measure the effect of the material in the shell and the ejecta. We flatten the ejecta-only and shell-only spectra using a continuum from the photosphere temperature and velocity, then identify the point of minimum flux of the CaNIR feature for the shell, which we refer to as the HVF velocity, and ejecta, which we refer to as the PVF velocity. We report these velocities in Figure 3, with the SN 2011fe PVF and HVF velocities from Parrent et al. (2012) and Silverman et al. (2015) shown for reference.

The IF is identified by visual inspection of the ejecta-only spectra generated from the SN+S model. At times before -7.27 d, where there are multiple small features blue-ward of the CaNIR minimum, we chose the feature that had a wavelength range similar to the IF on the successive epoch. We find a local minimum in the flux at the IF and report that velocity in Figure 3.

Comparing the HVF, PVF and IF velocities in this work to those of Parrent et al. (2012) and Silverman et al. (2015) requires recognition of the differing methods for velocity measurement. Parrent et al. (2012) report the v_{min} parameter they use for a `SYNAPPS` fit, which is equivalent to our photospheric velocity for the ejecta, but we have no equivalent for the shell other than the velocity of the contact discontinuity. Silverman et al. (2015) use a central velocity from a Gaussian profile line–fitting routine, which should be similar to our measured velocity, though some difference can be expected because the bottom of the CaNIR feature is not smooth.

At the earliest times, the photosphere is in the shell so the SN+S model has only a HVF and no measurable PVF, although a PVF is identified by both Parrent et al. (2012) and Silverman et al. (2015). The use of the v_{min} parameter by Parrent et al. (2012) can falsely suggest the presence of a PVF that is absent due to very low effective optical depths. The method for identifying PVF and HVF used by Silverman et al. (2015) and others may artificially require a two component fit because of the non-Gaussianity of the spectral feature as well as the choice of the P Cygni peak as the basis for the red–ward continuum. The similarity of the velocities produced by the `SYNAPPS` and Gaussian-fitting methods at the early times cannot be discounted, however our model results call for deeper consideration of the techniques used to characterize the early data.

The SN–O model produces a PVF with a velocity that is higher than the PVF velocity identified by Parrent et al. (2012) and Silverman et al. (2015) by about $5,000\ \mathrm{km\,s^{-1}}$ at -10.17 d and earlier, but is too slow to explain the HVF. The PVF velocity of the SN+S model agrees with that of Parrent et al. (2012) and Silverman et al. (2015) on the first day that it is measurable (-13.21 d), but remains at about the same velocity over the following six days. At the latest times, it is again in very good agreement with Parrent et al. (2012) and Silverman et al. (2015).

To explain the HVF in Parrent et al. (2012) and Silverman et al. (2015), we suggest that the observationally–identified HVF is generated by the shell at the earliest times (-10.54d and earlier) and by the IF at later times. Our HVF velocity is about $3,000\ \mathrm{km\ s^{-1}}$ slower than their HVF velocities during the shell-dominated phase; a slightly lower mass shell may explain the discrepancy, or it may be a result of the differing velocity measurement methods. We will further explore the effect of the mass of the shell in our upcoming paper Mulligan & Wheeler (in preparation).

4.2. Implications for progenitor models

Our results disfavor progenitor models that predict, or are consistent with, very little CSM. Models in this category could be spin–up / spin–down models in which mass transfer has long since ceased (Di Stefano et al. 2011; Di Stefano & Kilic 2012; Justham 2011) or models in which isolated white dwarfs explode by pycnonuclear reactions (Chiosi et al. 2015). In the absence of a CSM,

TABLE 1

PARAMETERS AND VARIANCE OF FIT

Model	MJD[a]	Phase[b]	Photosphere velocity (1000 km s^{-1})	Photosphere temperature (1000 K)	log C^E	log C^S	log σ
SN-O	797.66	-16.54	24.80	8.42	1.98	...	-1.73
	798.76	-16.24	22.26	8.00	1.14	...	-1.60
	800.69	-13.21	17.97	8.00	0.43	...	-1.89
	801.24	-12.66	19.58	11.76	0.06	...	-2.14
	803.36	-10.54	19.85	9.14	-0.30	...	-2.31
	803.73	-10.17	19.30	8.00	-0.81	...	-1.93
	806.63	-7.27	11.95	8.71	-1.90	...	-2.53
	811.73	-2.17	9.39[c]	19.55[c]	-2.17	...	-3.16
	816.77	2.87	5.97[c]	22.52[c]	-2.12	...	-2.76
SN-S	797.66	-16.54	21.66	8.01	...	0.41	-2.32
	798.76	-16.24	20.82	8.00	...	0.08	-1.65
	800.69	-13.21	18.35	8.03	0.12	-0.27	-1.72
	801.24	-12.66	16.98	10.19	-0.45	-0.60	-1.82
	803.36	-10.54	18.59	8.18	0.09	-0.91	-2.21
	803.73	-10.17	17.88	8.00	-1.33	-1.63	-1.81
	806.63	-7.27	19.09	8.47	-0.29	-2.72	-2.43
	811.73	-2.17	7.34[c]	18.90[c]	-2.39	-3.05	-3.19
	816.77	2.87	7.97[c]	22.81[c]	-2.18	-4.11	-2.79

[a] Relative to JD 2,455,000.5.

[b] Relative to B-band maximum on MJD 813.90 (Vinkó et al. 2012).

[c] The photosphere is at a velocity that is interior to all of the freshly–synthesized Ca and thus the velocity is not well constrained by this fit. The high temperature is a result of the low velocity.

these models would not produce HVF by the mechanism modeled here.

An important category of SN Ia explosion models involve edge–lit double detonations whereby the explosion is triggered in a sub–Chandrasekhar white dwarf by the detonation of a thin layer of He on the outside of a C/O core. The required mass of He is estimated to range from ~ 0.05 to $\sim 0.1 M_\odot$ (Fink et al. 2010; Woosley & Kasen 2011), although the mass of He might be considerably less if the He is enriched with C/O (Shen & Moore 2014). In the context of the current models, we note that the high-velocity ejection of such a He shell is unlikely to produce an observed HVF because the velocity will be too high and the optical depth too low.

Some progenitor model components can also be discounted as sources of the CSS. A thin accretion disk with a small solid angle would not account for the ubiquity of the HVF and such disks are typically much less massive than the shell that we have invoked. A steady-state wind would result in excess optical light, which is not observed (Gerardy et al. 2004), and would contain substantially less mass than does the shell presented here. The CSS may be a result of a thick disk or other phenomenon. Investigation into the composition of the CSS will provide insight into these sources.

5. Conclusion

We have compared the synthetic spectra from a model with only supernova ejecta (SN–O) and a model with the supernova ejecta colliding with a circumstellar shell of mass $0.005 M_\odot$ (SN+S) to the observed Ca II near–infrared triplet (CaNIR) feature in SN 2011fe (Parrent et al. 2012). The SN+S model generally produces a better fit to the width of the feature than the SN–O model. The SN+S model spectra and observations of SN 2011fe have a sub–feature near 8000 Å at late times which is absent in the SN–O model spectra. This feature, which we dub the interaction feature (IF), is a result of the interaction between the ejecta and the shell in our model.

The combination of the shell–HVF and IF in the SN+S model more consistently reproduces the observed HVF velocity evolution than does the SN-O model. The PVF velocity evolution in the SN+S model matches that of Parrent et al. (2012) and Silverman et al. (2015) when it first appears in this model and again near Bmax, but is about $2,000 \ \ \mathrm{km\ s^{-1}}$ fast at intermediate times. The SN–O model fails to account for either the HVF or the PVF velocity at any time before about -8d, and accounts for only the PVF velocity after this epoch.

We have made a plausible case that a shell of mass $\sim 0.005\, M_\odot$ accounts for the common presence of HVF in SN Ia. Discrepancies between the spectra generated by our models and the observed SN 2011fe features may be improved by using a more finely tuned mass or structure of the shell. Fitting of additional absorption features is necessary to place constraints on the physical quantities of the shell, such as the geometry, mass, and composition. These quantities will give us insight into possible origins of the shell and the cause of Type Ia supernovae.

Special thanks to Jeffrey Silverman, Howie Marion, and Jozsef Vinkó for many discussions about high–velocity features and the fits shown in this paper. Thanks to Vadim Gamezo for providing the source model of the post-explosion supernova. This work was supported in part by NSF grant AST-1109801. The Texas Advanced Computing Center (TACC) at the University of Texas at Austin has provided HPC resources that have contributed to the research results reported within this letter.

REFERENCES

Childress, M. J., Filippenko, A. V., Ganeshalingam, M., & Schmidt, B. P. 2014, MNRAS, 437, 338

Chiosi, E., Chiosi, C., Trevisan, P., Piovan, L., & Orio, M. 2015, MNRAS, 448, 2100

Di Stefano, R., Voss, R., & Claeys, J. S. W. 2011, ApJ, 738, LL1

Di Stefano, R., & Kilic, M. 2012, ApJ, 759, 56

Foley, R. J. 2013, MNRAS, 435, 273

Fink, M., Röpke, F. K., Hillebrandt, W., et al. 2010, A&A, 514, AA53

Fryxell, B., Olson, K., Ricker, P., et al. 2000, ApJS, 131, 273

Gamezo, V. N., Khokhlov, A. M., & Oran, E. S. 2005, ApJ, 623, 337

Gerardy, C. L., Höflich, P., Fesen, R. A., et al. 2004, ApJ, 607, 391

Hatano, K., Branch, D., Fisher, A., Baron, E., & Filippenko, A. V. 1999, ApJ, 525, 881

Justham, S. 2011, ApJ, 730, LL34

Kasen, D., & Plewa, T. 2005, ApJ, 622, L41

Maguire, K., Sullivan, M., Pan, Y.-C., et al. 2014, MNRAS, 444, 3258

Maguire, K., Sullivan, M., Ellis, R. S., et al. 2012, MNRAS, 426, 2359

Marion, G. H., Vinko, J., Wheeler, J. C., et al. 2013, ApJ, 777, 40

Mazzali, P. A., Benetti, S., Altavilla, G., et al. 2005, ApJ, 623, L37

Mulligan, B. W., & Wheeler, J. C. In preparation.

Nugent, P. E., Sullivan, M., Cenko, S. B., et al. 2011, Nature, 480, 344

Parrent, J. T., Howell, D. A., Friesen, B., et al. 2012, ApJ, 752, L26

Perlmutter, S., Aldering, G., Goldhaber, G., et al. 1999, ApJ, 517, 565

Piro, A. L., & Nakar, E. 2014, ApJ, 784, 85

Quimby, R., Höflich, P., Kannappan, S. J., et al. 2006, ApJ, 636, 400

Riess, A. G., Filippenko, A. V., Challis, P., et al. 1998, AJ, 116, 1009

Seitenzahl, I. R., Ciaraldi-Schoolmann, F., Röpke, F. K., et al. 2013, MNRAS, 429, 1156

Shen, K. J., & Moore, K. 2014, ApJ, 797, 46

Silverman, J. M., Vinko, J., Marion, G. H., et al. 2015, arXiv:1502.07278

Thomas, R. C., Nugent, P. E., & Meza, J. C. 2011, PASP, 123, 237

Timmes, F. X., & Arnett, D. 1999, ApJS, 125, 277

Tsujimoto, T., & Shigeyama, T. 2012, ApJ, 760, L38

Vinkó, J., Sárneczky, K., Takáts, K., et al. 2012, A&A, 546, A12

Wang, L., Baade, D., Höflich, P., et al. 2003, ApJ, 591, 1110

Woosley, S. E., & Kasen, D. 2011, ApJ, 734, 38

This 2-column preprint was prepared with the AAS LaTeX macros v5.2.

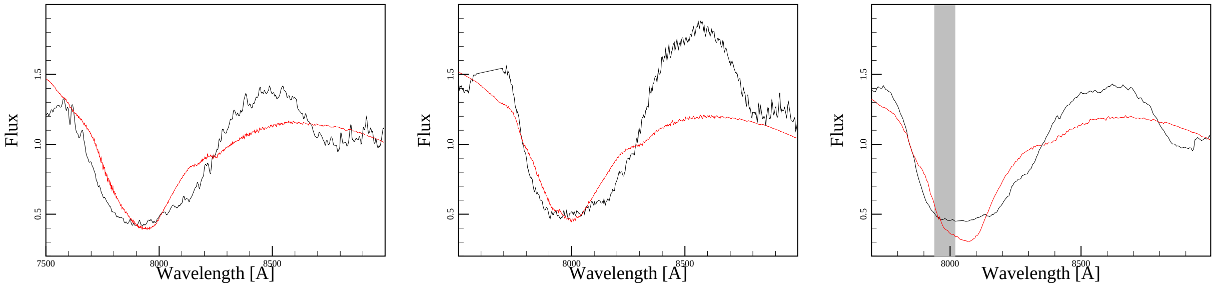

(a) −16.54 d (b) −15.24 d (c) −13.21 d

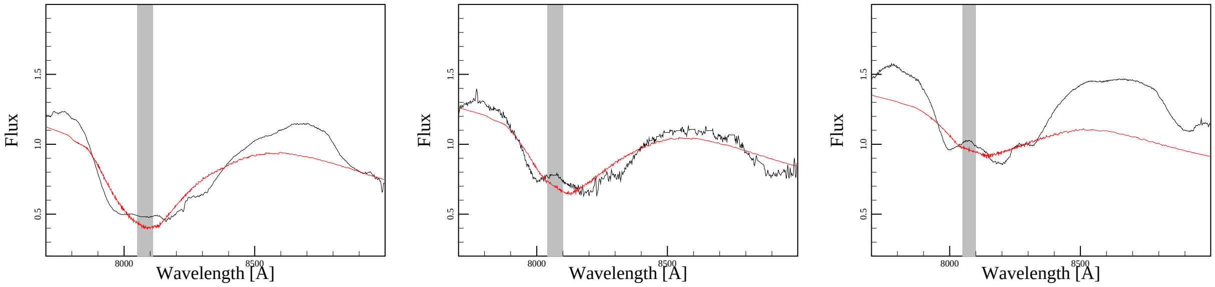

(d) −12.66 d (e) −10.54 d (f) −10.17 d

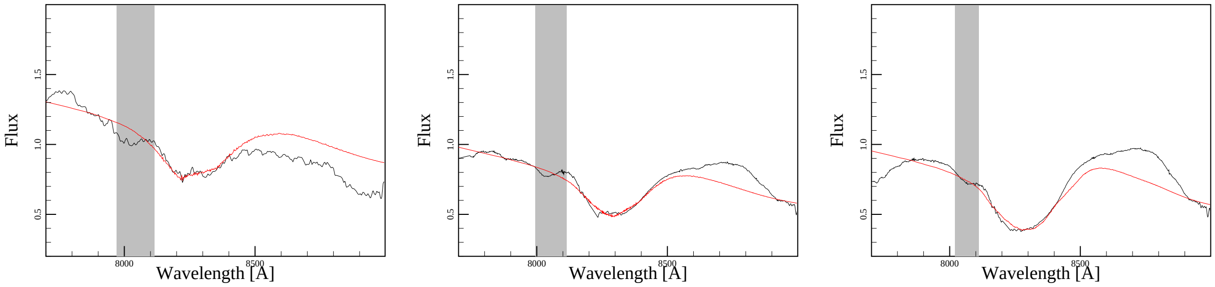

(g) −7.27 d (h) −2.17 d (i) +2.87 d

Fig. 1.— Results of fitting the CaNIR feature in the SN–O model to SN 2011fe. SN 2011fe spectra are shown in black (Parrent et al. 2012) and the generated spectrum from the model is shown in red. The gray shaded regions at −13.21 d and later represent the approximate range of the IF in the SN+S model spectra; there is no equivalent feature in the SN–O model spectra in these regions.

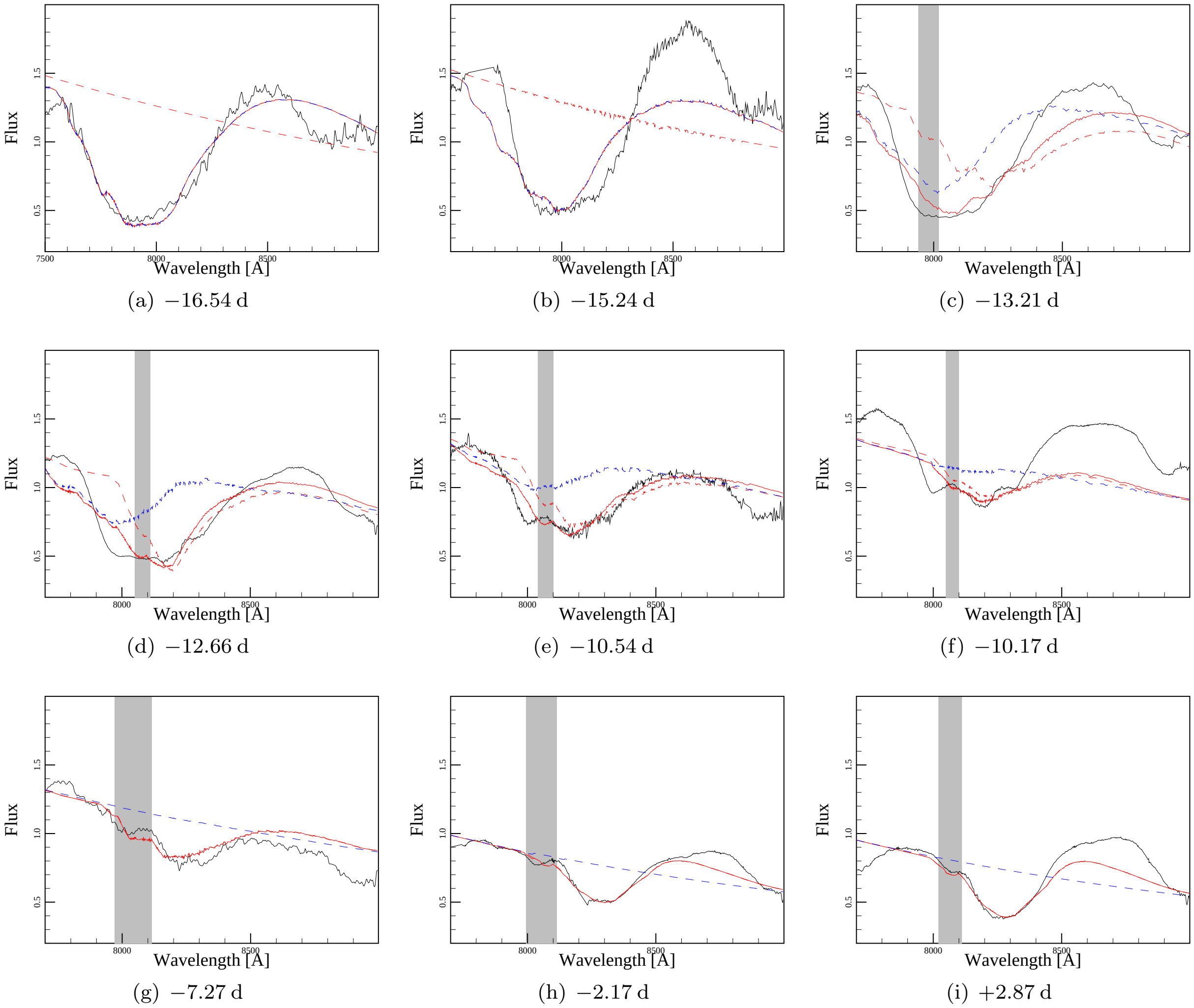

(a) −16.54 d (b) −15.24 d (c) −13.21 d

(d) −12.66 d (e) −10.54 d (f) −10.17 d

(g) −7.27 d (h) −2.17 d (i) +2.87 d

Fig. 2.— Results of fitting the CaNIR feature in the SN+S model to SN 2011fe. SN 2011fe spectra are shown in black (Parrent et al. 2012), the generated spectrum from the model is shown in solid red, a spectrum showing the effects of only the shell is shown in dashed blue, and that of only the supernova ejecta is shown in dashed red. At early and late times the ejecta and shell component of the spectrum, respectively, is shown as a continuum due to high photospheric velocity (early times) and thinning of the material (late times). The gray shaded regions at −13.21 d and later represent the approximate range of the IF in the SN+S model spectra.

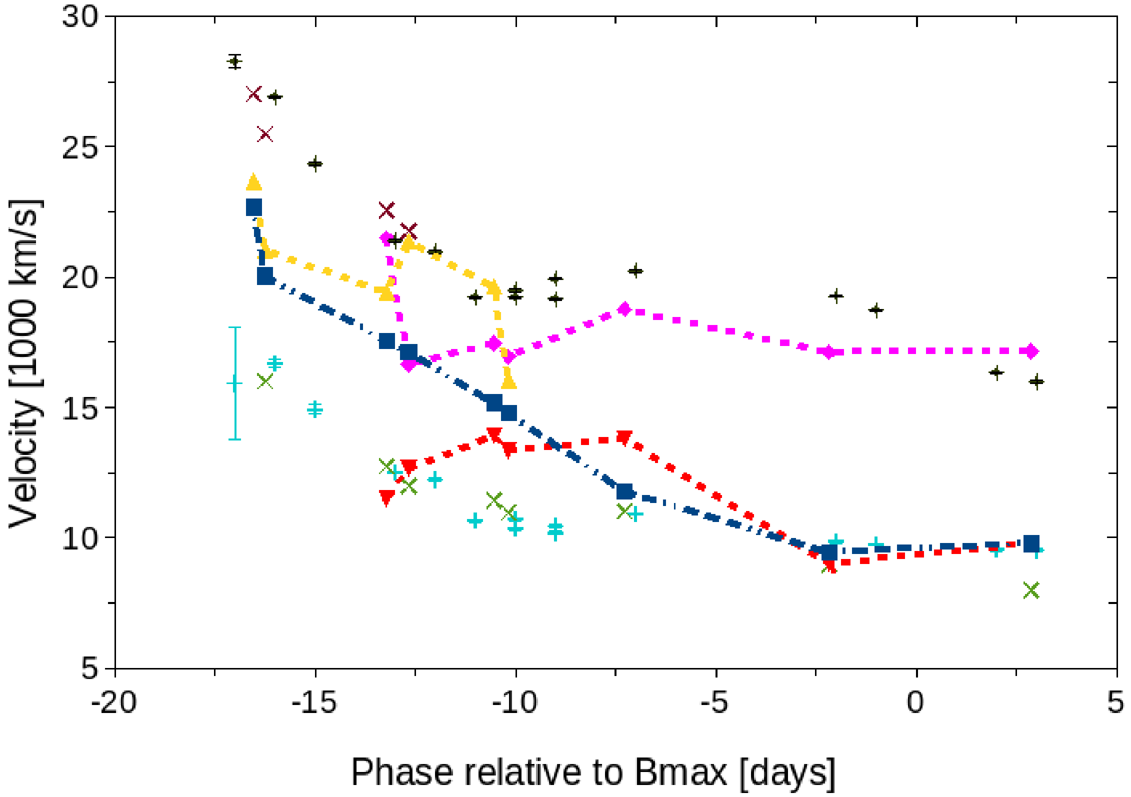

Fig. 3.— Evolution of the Ca II near IR triplet feature velocities for the SN–O model (blue, dash–dot, ■), the SN+S model (dashed, PVF: red, ▼; HVF: yellow, ▲; IF: magenta, ⧫), and the Ca II PVF and HVF velocities reported by Parrent et al. (2012) (×, PVF: green; HVF: brown) and Silverman et al. (2015) (+, PVF: cyan; HVF: dark brown). The Parrent et al. data stop at −10 d, but the Silverman et al. HVF velocities extend to Bmax where they correspond to the IF velocity in the SN+S model.